Journal of Multivariate Analysis 132 (2014) 1–8

Contents lists available at ScienceDirect

Journal of Multivariate Analysis

journal homepage: www.elsevier.com/locate/jmva

A contribution to the visualisation of three-way arrays

Casper J. Albers [a,*], John C. Gower [b]

[a] Department of Psychometrics & Statistics, University of Groningen, Groningen, The Netherlands
[b] Department of Mathematics & Statistics, The Open University, Milton Keynes, United Kingdom

ARTICLE INFO

Article history:
Received 10 March 2014
Available online 7 August 2014

AMS subject classifications:
62H25
15A72
62-07
00A66

Keywords:
Biplots
Candecomp decomposition
PARAFAC
Multiway data

ABSTRACT

Visualisations of two-way arrays are well-understood. Here, a procedure, with geometric underpinning, is given for visualising rank-two three-way arrays in two-dimensions.

1. Introduction

In the analysis of multiway tables, model-fitting, interpretation and visualisation of interactions are important phases. Much of the standard exposition is based on linear models, generalised linear models [16], or generalised additive models [11]. In all such models, the estimation of additive parameters, which may include additive interaction terms, is well understood, but they are not conducive to visualisation. As early as [5], multiplicative/additive parametrisations were considered but because of computational limitations it was not until the computer revolution that they became popular, especially in genotype–environment studies. The estimates of biadditive model multiplicative parameters are routinely visualised in maps of two sets of points; one arising from the row-parameters and the other from the column-parameters. These biplot maps greatly help the interpretation of interactions between two factors. Usually, such maps are two-dimensional; though higher dimensional biadditive fits are easy to compute they are less easy to interpret by visual inspection. For a brief discussion of the term biadditive and its extension to triadditive as used below, see [4].

Here we discuss one possibility for mapping three-factor multiplicative interactions. As with visualisations of two-way arrays, our methods are rooted in Euclidean geometry, orthogonal projections and calibrated axes. Reference to these topics and their mathematical derivations can be found in, e.g., [15,7]. Consider a decomposition of a three-way array $\mathbf{X} = \{x_{ijk}\}$ $(i = 1, \ldots, I; j = 1, \ldots, J; k = 1, \ldots, K)$:

$$x_{ijk} = \sum_{r=1}^{R} u_{ir} v_{jr} w_{kr} \tag{1}$$

which has the form of a Singular Value Decomposition of a matrix generalised to three-way arrays, although crucially without its nice orthogonal least squares properties.

* Corresponding author.
E-mail address: c.j.albers@rug.nl (C.J. Albers).

http://dx.doi.org/10.1016/j.jmva.2014.07.013
0047-259X/

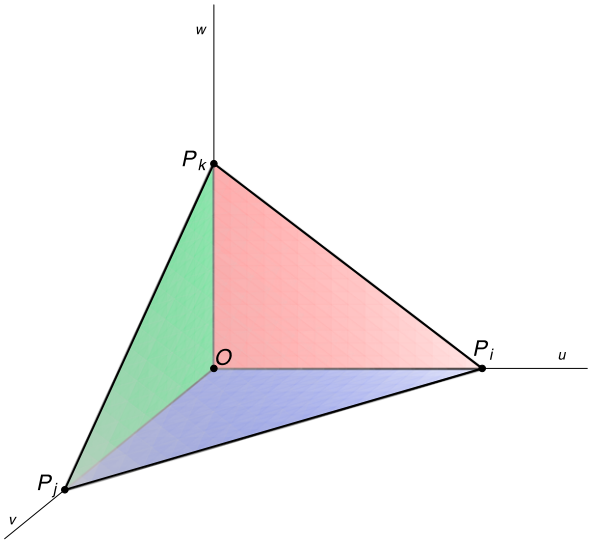

Fig. 1. Rank one visualisation in three dimensions. The value x_{ijk} is the volume of the tetrahedron with vertices O, P_i, P_j, P_k.

We adopt the terminology introduced by [14] of referring to a decomposition (1) as having rank R when it cannot be written in fewer terms. A growing literature on three-way rank has been summarised by [18], though it has little overlap with this paper. The basic algorithm for fitting (1) was independently due to [2,10], who termed it Candecomp and PARAFAC, respectively, although the basic idea goes back 43 years earlier [12]. Examples of the varieties of ways that three-way arrays may arise in applications can be found in [13,17]. Here, the neutral term "array" is used as an omnibus term to cover cross-classified tables, sets of data-matrices, configuration matrices and other three-way constructs. A three-way array $\mathbf{X}$ may represent raw data, or it may have been derived as an approximation to raw data, or it may be a term in some, possibly extensive, model. Thus, although one could analyse any rank-2 three-way array as raw data, often some preprocessing is required, as in our example below. All we seek here is a good visualisation of $\mathbf{X}$, however it may have been derived.

We define $\mathbf{U}$ with columns $\{\mathbf{u}_i\}$, $\mathbf{V}$ with columns $\{\mathbf{v}_j\}$, and $\mathbf{W}$ with columns $\{\mathbf{w}_k\}$, each with R columns. For reasons made clear below, we assume without loss of generality that $I \leq J \leq K$. Although matrices written $\mathbf{U}$ and $\mathbf{V}$ are often associated with expositions of the SVD, expressed in orthogonal forms, we emphasise here that no such restrictions apply in the following.

The paper is structured as follows. Section 2 gives (i) details of what is required for computations and (ii) the geometric and algebraic underpinning. Section 3 gives an example of our method and we finish with a discussion in Section 4.

2. Visualisation

It is clear from the previous section that visualisation is important in the interpretation of two-way arrays. Below, we explore to what extent three-way arrays may be visualised in two dimensions.

2.1. Basic method

In the rank one case ($R = 1$), the points for u_{i1} $(i = 1, \ldots, I)$; v_{j1} $(j = 1, \ldots, J)$; w_{k1} $(k = 1, \ldots, K)$ may be placed on separate orthogonal coordinate axes, which we shall label u, v and w. Then, $x_{ijk} = u_{i1}v_{j1}w_{k1}$ is simply proportional to the volume of the tetrahedron with the three points $P_i = (u_{i1}, 0, 0)$, $P_j = (0, v_{j1}, 0)$, $P_k = (0, 0, w_{k1})$ and the origin as vertices cf. [7], as shown in Fig. 1.

When $R = 2$, we may inspect the two-dimensional sets of coordinates U, V and W but this ignores intrinsic three-way information. Then, one way of proceeding is to write

$$x_{ijk} = u_{i1}v_{j1}w_1 + u_{i2}v_{j2}w_2 \tag{2}$$

where (w_1, w_2) takes on the values (w_{k1}, w_{k2}) as k varies in the range $(1, \ldots, K)$ while i and j remain fixed. The line represented by (2) may be envisaged in the two-dimensional plane of the K coordinates comprising the rows of $\mathbf{W}$. We term

$$(u_{i1}v_{j1})w_1 + (u_{i2}v_{j2})w_2 = 0$$

the *zero line*. The (Euclidean) distance of any point (w_{k1}, w_{k2}) from the zero line is

$$\kappa_{ij}(u_{i1}v_{j1}w_{k1} + u_{i2}v_{j2}w_{k2})$$

which is proportional to the required triadditive form with $R = 2$. The factor κ_{ij} ensures that the coefficients of (w_1, w_2) are normalised in the form of direction-cosines, as is required, and is given by $\kappa_{ij}^{-2} = (u_{i1}v_{j1})^2 + (u_{i2}v_{j2})^2$. When different values k' are used, the lines (2) remain parallel, i and j remaining fixed. The distance from the zero line increases with x_{ijk}. When

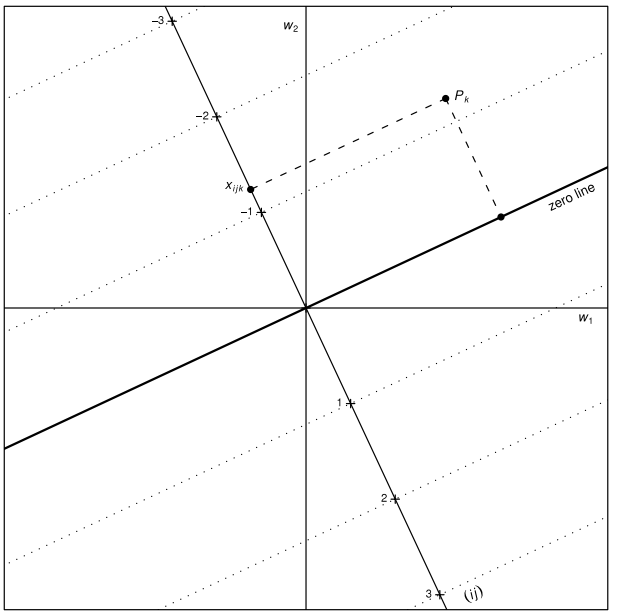

Fig. 2. The zero line through the origin with parallel lines at one unit of x_{ijk} apart (i, j fixed). A line orthogonal to the zero line gives the calibration for i, j. A point (w_{k1}, w_{k2}) projects onto the calibration axis to give the correct value of x_{ijk}.

$P_{k'}$ is on the zero line itself, the distance is zero. On either side of the zero line, depending on the sign of x_{ijk}, the distance increases positively on one side and negatively on the other side. All IJ settings P_i, P_j of the first two factors will give a set of linear axes through the origin O, in the plane of the points $\mathbf{W}$, as is visualised in Fig. 2. Thus, calibration points may be taken on an axis through the origin that is orthogonal to the zero line and so has equation:

$$(u_{i2}v_{j2})w_1 - (u_{i1}v_{j1})w_2 = 0. \tag{3}$$

The intersection of (2) and (3) gives a point C with coordinates $x_{ijk}\kappa_{ij}^2(u_{i1}v_{j1}, u_{i2}v_{j2})$ which may be calibrated with the value x_{ijk} for as many points on (2) as are found convenient. Thus, values of x_{ijk} are assessed in the usual way by orthogonal projection from instances of $P_k(w_{k1}, w_{k2})$ onto the calibrated axis generated by i and j, as is shown in Fig. 3. Such calibrated axes are essentially the same as the familiar $x - y$ axes used in many fields of application and may be used in the same way, except that the axes generated by different settings of i and j are oblique.

Rather than the plane W, the above procedure may be based on the planes determined by U or V but they would give the same predictions. Because $I \leq J \leq K$, the use of W has the advantage that it generates only IJ axes which is fewer than IK or JK required by the other two options. Nevertheless, even IJ may generate many axes and ways of selecting the more salient may be sought, perhaps through circular projection (see Fig. 3 and Section 3), or by interactive inspection, or as guided by external knowledge. Recall that circular projection is a simple way described by [9] for simultaneously showing the orthogonal projections from a point P onto n axes, as the intersections of the circle on diameter PO with the axes—it depends on the property that diameters subtend right angles on the circumference. Its advantage is that one circle gives the same information as K orthogonal projections as is shown in Fig. 3.

2.2. Geometrical foundations

Although the arrays $\mathbf{U}$, $\mathbf{V}$ and $\mathbf{W}$ may be individually analysed and visualised, they are linked only through the algebraic formula (1). The graphical method described in Section 2.1 allows the evaluation of (1) given the values of $\mathbf{U}$, $\mathbf{V}$, and $\mathbf{W}$ but gives no visual understanding in terms of geometric concepts in the way, that using concepts such as distance, area and inner-products, have been found so valuable for two-way arrays. In the following we make some suggestions for addressing this problem.

Further light may be thrown on the process given in Section 2.1 by noting that, when $R = 2$, a visualisation may be derived from the following simple result:

$$x_{ijk} = u_{i1}v_{j1}w_{k1} + u_{i2}v_{j2}w_{k2} = \det\begin{pmatrix} 0 & u_{i1} & u_{i2} \\ v_{j2} & 0 & v_{j1} \\ w_{k1} & w_{k2} & 0 \end{pmatrix}. \tag{4}$$

Conforming to the structure of (4) we now redefine:

$$\mathbf{U} = (\mathbf{0},\ \mathbf{u}_1,\ \mathbf{u}_2), \qquad \mathbf{V} = (\mathbf{v}_2,\ \mathbf{0},\ \mathbf{v}_1), \qquad \mathbf{W} = (\mathbf{w}_1,\ \mathbf{w}_2,\ \mathbf{0}) \tag{5}$$

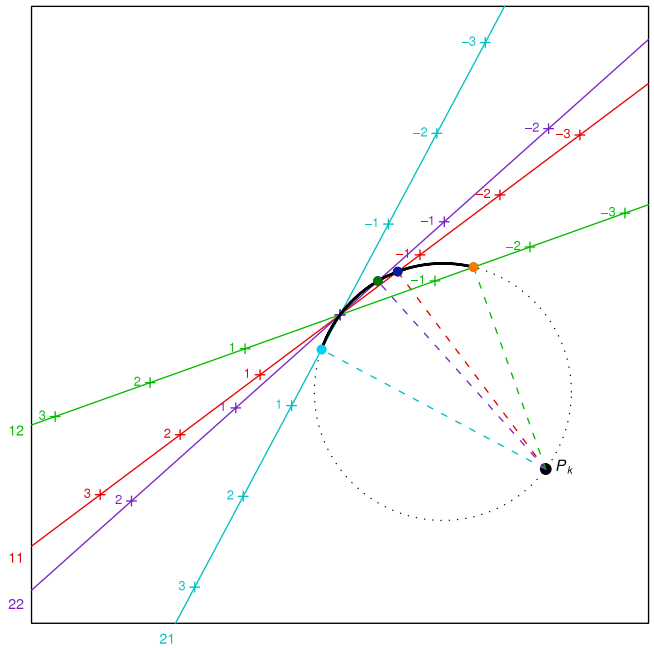

Fig. 3. Calibrated axes give all IJ (11, 12, 21, 22) settings of x_{ijk}. A circular arc highlights the active region for the setting of k shown; other settings of k share the same calibration axes but give different circles. The dotted lines show the ability of the diameter OP_k to give simultaneous orthogonal projections; these would not be shown in practice.

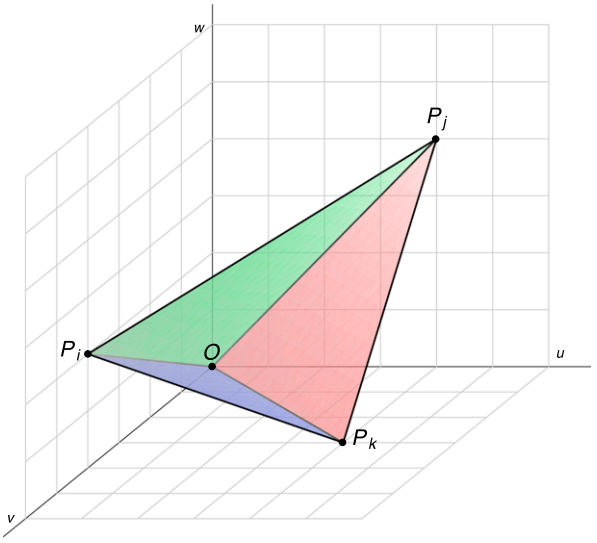

Fig. 4. Rank two visualisation in three dimensions. The value x_{ijk} is the volume of the tetrahedron with vertices O and P_i, P_j, and P_k where each vertex is chosen from one of the u- v- and w-planes.

where the two-dimensional structure of each matrix is preserved but now set in three dimensions. We name these coordinates u, v, w even though the U-plane has $u_1 = 0$ and in general u_2 and u_3 are non-zero; similarly for the other axes. Thus, for example, the points ($\mathbf{w}_1$, $\mathbf{w}_2$, $\mathbf{0}$) of $\mathbf{W}$ lie entirely in the uv-plane.

The determinant in (4) is three times the volume of the tetrahedron defined by the origin and the three-dimensional coordinates given by the rows of the matrix, showing that rank 2 three-way arrays may be represented by volumes of single tetrahedra. We may set in three dimensions the points (P_1, P_j, P_k) whose coordinates are obtained conformally from the rows of the matrix in (4) arising from all i, j, and k settings, as shown in Fig. 4.

Thus, rank-two three-way arrays have a Euclidean representation in three dimensions but constrained to lie on three orthogonal planes. Such figures are hard to interpret. Note that the rank-one visualisation of Fig. 1 is a special case of the rank-two visualisation where the configurations in the plane faces collapse into the axes.

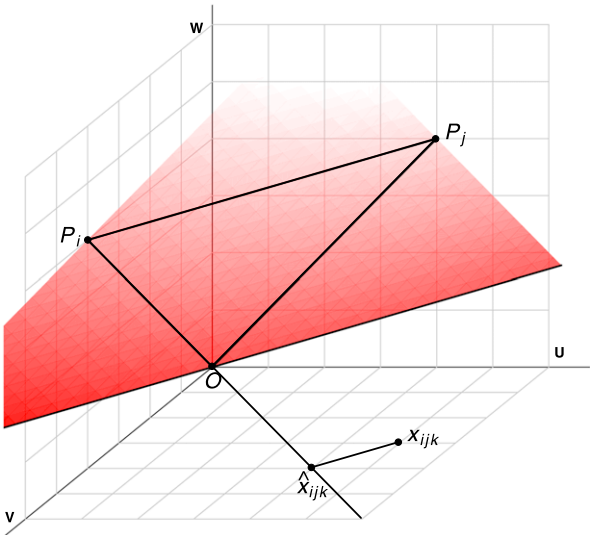

Fig. 5. The geometry shows how the plane OP_iP_j intersects with the u, v plane to give the zero line and its orthogonal calibrated axis that gives values of x_{ijk} by orthogonal projection.

The above is similar to, but less accessible than, what has been found useful for biadditive models. Even with two-way arrays it is rare for published displays to be shown in more than two-dimensions, so it seems likely that, if available, rank two approximations to three-way arrays should suffice for many purposes, especially if they can be accurately visualised in two Euclidean dimensions as we shall describe. Note that unlike two-way arrays where rank and dimensionality are closely linked, for three-way arrays the link is looser. To represent rank-two three-way arrays, in the above, we have found it necessary to use three Euclidean dimensions.

Despite the simplification given by the constrained orthogonal-plane structure, a tetrahedronal visualisation such as that of Fig. 4, is not conducive to easy interpretation. Progress can be made as follows. Firstly, we concentrate on the separate planes $u = 0$, $v = 0$, $w = 0$ and, in particularly, on $w = 0$ and note that the plane OP_iP_j: $(u_{i1}v_{j1})w_1 + (u_{i2}v_{j2})w_2 = w$ intersects $w = 0$ in the line:

$$(u_{i1}v_{j1})w_1 + (u_{i2}v_{j2})w_2 = 0$$

which is the zero line defined in Section 2.1. The geometry is shown in Fig. 5.

The position is precisely the same as that discussed in Section 2.1 and visualisation in two dimensions follows in precisely the same way and, as before, we continue to focus on the plane $w = 0$ because it uses fewer linear axes. Without any approximation, the two-dimensional visualisation in the plane $w = 0$ gives a precise description of any rank two three-way array.

The three-dimensional Euclidean representation of this section gives geometrical understanding that underpins the procedure given in Section 2.1. In particular, because volume is invariant to orthogonal transformations, one may deduce from the Euclidean representation that the parameters of rank 2 three-way arrays are determined at most only up to arbitrary orthogonal rotations (excluding reflections) in three dimensions. This degree of arbitrariness is similar to that found with inner-products where areas and inner-products, rather than volume, are the appropriate invariants. However, orthogonal transformation is not the only invariant for rank 2 triadditive models; for example, provided $\alpha\beta\gamma = 1$, we could also scale axes by α, β and γ without affecting volume (see e.g. the example in Section 3). Moreover, the matrix (4) may be post-multiplied by any rank-three matrix $\mathbf{A}$, where $\det \mathbf{A} = 1$, without affecting content and this extends to the matrices $\mathbf{U}$, $\mathbf{V}$, and $\mathbf{W}$ defined in (5). Hence all estimates of x_{ijk} are invariant to such transformations. With this degree of arbitrariness, special attention has to be given to any attempt to interpret the individual estimated values of the parameters u, v, w. It is better to focus on the invariants, such as volume and the actual fitted values $\hat{x}_{ijk}$. This is what our visualisation does.

3. Example

Now, we shall apply our theory to a concise set of three-way data given in [3, Example 8.1]. A $3 \times 4 \times 5$ table arises from a study of the effects of three factors on the measurements of the wearing performance of vulcanised rubber. The three factors considered are:

- Factor A. The method of pre-treatment of the rubber ($I = 3$)
- Factor B. The quality of the raw rubber ($J = 4$)
- Factor C. The quality of filler ($K = 5$ levels)

The main effects of the factors are huge, so we confine our interest to the interactions between factors; that is after removing the main effects from the original table. Table 1 gives the data (i) in its original form and (ii) after main effects have

Table 1
Rubber wear classified by three factors from [3] in (i) original form (top) and (ii) after removing main effects (bottom).

Level of factor C	Level of factor A											
	1				2				3			
	Level of factor B				Level of factor B				Level of factor B			
	1	2	3	4	1	2	3	4	1	2	3	4
1	404	478	530	381	429	528	316	376	390	423	482	550
2	392	239	186	410	418	251	207	416	431	249	194	452
3	348	327	290	383	381	372	315	376	460	482	350	496
4	296	165	158	301	291	232	279	306	333	242	220	330
5	186	129	105	213	198	157	163	200	225	197	190	255
1	−41.15	1.92	−20.35	−36.95	−0.90	16.17	5.90	−11.70	12.25	76.32	−18.95	17.45
2	67.02	−19.92	−30.18	70.22	59.27	−41.67	−42.93	42.47	33.42	−892.52	−94.78	39.62
3	−38.23	6.83	12.57	−18.03	−38.98	18.08	3.82	−58.78	1.17	89.23	−0.03	22.37
4	28.68	−36.25	−0.52	18.88	−10.07	−3.00	86.73	−9.87	−6.92	−31.85	−11.12	−24.72
5	−3.40	5.67	24.40	8.80	−25.15	−0.08	48.65	−37.95	−37.00	1.07	36.80	−21.80

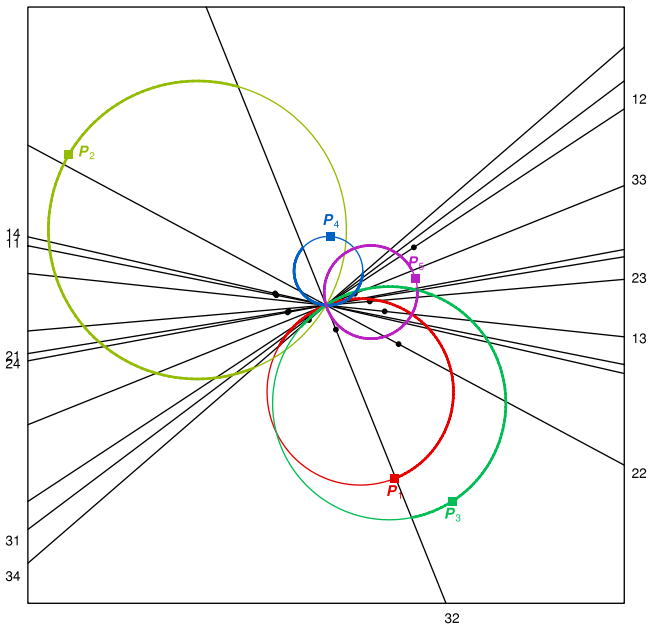

Fig. 6. Two-dimensional diagram of the $3 \times 4 \times 5$ data of [3] with main effects eliminated. The labels of the first two factors are given in the margins, at the positive end of each axis. The levels of the third factor are depicted as the set of points $P_1, \ldots, P_5$. A single calibration point of value 10 units of wear is shown on each axis as a small black dot. Projection circles with OP_k as diameter are provided. The active arcs of the projection circles are highlighted.

been removed. Subsequently, a rank $R = 2$ Candecomp decomposition is performed, which covers 75% of the variance in the table. The matrices **U**, **V**, and **W** given by Candecomp were redefined as $\alpha\mathbf{U}$, $\beta\mathbf{V}$, $\gamma\mathbf{W}$, which can be done without affecting the visualisation, as long as $\alpha\beta\gamma = 1$. The rescaling is arranged such that the mean absolute values of **U**, **V**, and **W** coincide, so giving a balanced representation. For each combination of i and j, $IJ = 12$ linear axes were constructed and points P_k were plotted (Fig. 6). The axes may be calibrated (see Section 2.1) but, to reduce clutter, in Fig. 6 we show just one calibration marker on each axis. Values of x_{ijk} are assessed in the usual way by orthogonal projection from instances of the points P_k onto the calibrated axes generated by i and j and interpolating between the calibration markers. Because these projections are orthogonal, the circle C_k with OP_k as diameter passes through all these projections. This is termed circular projection by [9] and is useful for example in exhibiting a circular arc that exhibits sequentially all the values for rows ($i = 1, \ldots, I$) and columns ($j = 1, \ldots, J$) associated with P_k. Circular projections are shown in Fig. 6 and may be used to assist in interpretation.

Thus, as an example of how to use Fig. 6, consider x_{212} for which $i = 2, j = 1$ and $k = 2$. This is given by the projection of P_2 onto the 21 axis, which is made easy by using the projection circle with diameter OP_2 and its intersection with the 21 axis. To give the numerical value, one also has to take into account the calibration marker (positive in this case but negative when the marker is on the other side of the origin to the projection). The size of the chord OP_k is relative to its calibration point. An extreme instance of this is given by x_{332} where the calibration point for axis 33 almost coincides with the origin showing that x_{332} has a numerical value far from zero (−892 in Table 1).

The circles with OP_1 and OP_3 as diameters are similar in size and location so will have similar interactions with the factors. The circle for P_2 is bigger and separate from the first two circles and so has a different set of interactions. The circles on P_4 and P_5 are smaller and so their factors have less interaction with the other factors. By construction the axes all pass through the origin but axes that are close to being tangential at the origin will tend to have the smaller interactions. This remark is not absolute because each axis is separately calibrated but in this example, at least, the differences in calibration are small, Thus, interaction sizes can be safely compared. The worst cases are for factor-pairs 12 and 22 which are somewhat larger but not dramatically so. Thus, the circle for P_2 is tangential to most of the other factors and has large interactions, both positive and negative, as well as zero, not shared with the other factors. Similarly there are other factors that have large but different signs from those of P_2.

This analysis is not exhaustive but suffices to show that the visualisation has considerable structure and is able to convey a vast amount of information.

In summary, the visualisation shows (i) how the axis for levels (I, J) gives the magnitude of the interaction of rubber wear for each of the levels of factor C, and (ii) the same thing can be done for comparing the levels (I_i, J_j) and $(I_{i'}, J_{j'})$ on two axes, taking into account any differences there may be in the calibration of both axes and (iii) the intersections of the projection circles with the axes are useful for drawing attention to the large or small interactions and their signs and (iv) the intersection circles indicate how the sizes of interactions vary regularly with the different combinations of levels (I, J) around the circumferences.

4. Discussion

For clarity, in Section 3 we chose data with few factor levels. However, the theory could equally well be applied to more voluminous datasets (see, e.g., [1]), although too large values of I, J and/or K will tend to yield graphical overload. Nevertheless, a relatively quick look at Fig. 6 already provides vast information on the interactions in the data, the factor levels that are most similar, etc. Even a small dataset such as this delivers an ANOVA table that is too large to quickly grasp its gist. We believe that our method can strongly help data understanding.

Rather than (1), the so-called Tucker3 model has sometimes been used to represent three-way arrays (see e.g. [19]). Although no doubt Tucker3 has its uses, we feel that it is less fundamental than (1) and, moreover, it includes a three-way "core" matrix which is itself a potential candidate for three-way visualisation.

We have made some progress in deriving precise two-dimensional plots for rank-two three-way arrays. This visualisation gives points in two-dimensions displayed on three orthogonal planes, one for each factor. Each of the three faces could be shown separately but we have shown how the three-dimensional configurations of the u and v-planes may be characterised in the w-plane, without loss of information, to give a two-dimensional biplot-type of representation of all the elements of $\mathbf{X}$. When IJ is large this display may become overloaded and some of the methods we have briefly discussed, may be used to exclude inessential information. It should be realised that in Fig. 6 we have been tempted to show everything that could potentially be of use. In an interactive computer environment one would zoom in on areas of interest, select axes and points of marginal interest for deletion, and refine the intervals of calibration.

Rank-two three-way arrays are plagued by the disparity between rank (here $R = 2$) and dimensionality and this disparity has been at the heart of the above discussion. Higher rank solutions are worth examining. For example, it would be convenient if a direct visualisation of a rank-three three-way array could be developed. To this end we extend the method described in Section 2.1 for rank-two three-way arrays to rank-three three-way arrays. With $R = 3$ Eq. (2) becomes

$$x_{ijk} = u_{i1}v_{j1}w_1 + u_{i2}v_{j2}w_2 + u_{i3}v_{j3}w_3$$

which, by fixing i and j gives a plane with normal direction-cosines $(u_{i1}v_{j1}, u_{i2}v_{j2}, u_{i3}v_{j3})$. As x_{ijk} varies, the planes remain parallel so, as before, their common normal may be used for calibrating x_{ijk}. However, now the calibrated axes are in three dimensions and would be difficult to develop for practical use.

More directly, higher rank solutions to three-way arrays can be shown by exhibiting several planar cross-sections of the higher dimensional space. For example, when $R = 4$ we may write $(u_{i1}v_{j1}w_{k1} + u_{i2}v_{j2}w_{k2}) + (u_{i3}v_{j3}w_{k3} + u_{i4}v_{j4}w_{k4})$, the sum of two rank-two terms each representable by a single tetrahedron. Similarly, we can get a rank three visualisation by combining a rank-two visualisation with a rank-one visualisation, which as we have seen is three-dimensional (Fig. 1). However, adding two or more volumes, is unacceptable but perhaps little more so than is adding extra dimensions to a principal components analysis.

We surmise that rank-two representations of three-way arrays are at the limits of useful graphical representation; higher rank visualisations are theoretically possible but are impracticable. Fortunately, as with two-way arrays, it is the rank-two displays that are the most useful.

If high rank graphical representation is doomed to failure, there remains the possibility that our approach may have some bearing on the search for canonical forms suitable for three-way arrays. The three orthogonal planes of the two-rank form, together with its rank-one specialisation, is geometrically attractive. It shows that $\mathbf{X}$ may always be decomposed into three-dimensional components each with special planar structure and each of which may be represented in two dimensions. This recalls the fundamental structure of how two-way arrays may be decomposed into the sum of rank-one matrices (either by spectral or singular value form). Of course, our three-way decomposition lacks the underpinning provided by optimal least-squares properties of matrix canonical forms but it is possibly worth considering that the three-planes two-rank

structure may be fundamental to the algebra of three-way arrays. Furthermore, we note the link between volume and area (see e.g. the area interpretations of inner-products discussed by [8]) and conjecture that higher order multi-additivity might be associated with higher order content.

Postscript

A referee has questioned the role of geometrical visualisations in the analysis of data. Of course, numerical methods of the analysis of multiway arrays are of great value, and presentation of such analyses in numerical form is a basic tool of statisticians. Indeed, an initial numerical analysis underpins what the visualisations visualise. Nevertheless, we think that graphical visualisations are valuable in at least three ways: (i) they give the opportunity of identifying properties of the data that are more easily seen in visual form, rather than by scanning columns of figures; and (ii) visualisations are a good way of presenting results in reports and other publications to be read by the general public and researchers in diverse fields of applications, where visualisations can supplement numerical material; and (iii) on a theoretical level, geometry throws light on properties of the model being fitted. In our view, it is not a question of whether to use numerical or visual methods: both are useful.

Note that a user of the results of this paper only has to know how to use a calibrated axis. To understand the underlying theory is also undemanding. One has to know the formula for a plane in three dimensions, its intersection with another plane (which is a line), the distance of a point from a line and how to calculate volume (in three dimensions) see, for instance, [7,15].

Software usage

All computations have been performed in R (www.cran-project.org), using self-written code (Available from www.casperalbers.nl). For the Candecomp-decompositions the package ThreeWay [6] has been used.

References

[1] C.J. Albers, J.C. Gower, S. Unkel, Triadditive models for three-way tables, submitted for publication.
[2] J.D. Carroll, J.J. Chang, Analysis of individual differences in multidimensional scaling via an *n*-way generalization of 'eckart-young' decomposition, Psychometrika 35 (1970) 283–319.
[3] O.L. Davies (Ed.), The Design and Analysis of Industrial Experiments, second ed., Oliver and Boyd, Edinburgh, 1960.
[4] J.B. Denis, J.C. Gower, Biadditive models, Biometrics 50 (1994) 310–311.
[5] R.A. Fisher, W.A. Mackenzie, Studies in crop variation II. the manurial response of different potato varieties, J. Agric. Sci. 13 (1923) 311–320.
[6] P. Giordani, H.A.L. Kiers, M.A. del Ferraro, Three-way component analysis using the R package ThreeWay, J. Statist. Softw. 57 (7) (2014) 1–23.
[7] J.C. Gower, Euclidean distance geometry, Math. Sci. 7 (1982) 1–14.
[8] J.C. Gower, P.J.F. Groenen, M. van de Velden, Area biplots, J. Comput. Graph. Statist. 19 (2010) 46–61.
[9] J.C. Gower, D.J. Hand, Biplots, Chapman and Hall, London, 1996.
[10] R.A. Harshman, Foundations of the PARAFAC procedure: models and methods for an 'explanatory' multi-mode factor analysis, UCLA Working Pap. Phonetics 16 (1970) 1–84.
[11] T.J. Hastie, R.J. Tibshirani, Generalized Additive Models, Chapman & Hall/CRC, Boca Raton, Florida, 1990.
[12] F.L. Hitchcock, The expression of a tensor or a polyadic as a sum of products, J. Math. Phys. 6 (1927) 164–189.
[13] P.M. Kroonenberg, Applied Multiway Data Analysis, Wiley, Hoboken, New Jersey, 2008.
[14] J.B. Kruskal, Three-way arrays. rank and uniqueness of trilinear decompositions with applications to arithmetic complexity and statistics, Linear Algebra Appl. 18 (1977) 95–138.
[15] K.T. Leung, S.N. Suen, Vectors, Matrices and Geometry, Hong Kong University Press, 1994.
[16] P. McCullagh, J.A. Nelder, Generalized Linear Models, second ed., Chapman & Hall/CRC, Boca Raton, Florida, 1989.
[17] A.K. Smilde, R. Bro, P. Geladi, Multi-way Analysis with Applications in the Chemical Sciences, John Wiley & Sons, Hoboken, New Jersey, 2004.
[18] J.M.F. ten Berge, Simplicity and typical rank results for three-way arrays, Psychometrika 76 (2011) 3–12.
[19] F.A. van Eeuwijk, P.M. Kroonenberg, Multiplicative models for interaction in three-way ANOVA, with applications to plant breeding, Biometrics 54 (1998) 1315–1333.